AGU PUBLICATIONS

Geophysical Research Letters

RESEARCH LETTER
10.1002/2014GL060868

Key Points:
- Meridional temperature gradient change is the main cause of HC strength change
- Meridional temperature gradient change explains intermodel spread of HC change
- The scaling relations predict the changes in HC strength fairly well

Correspondence to:
K.-H. Seo,
khseo@pusan.ac.kr

Citation:
Seo, K.-H., D. M. W. Frierson, and J.-H. Son (2014), A mechanism for future changes in Hadley circulation strength in CMIP5 climate change simulations, *Geophys. Res. Lett.*, *40*, 5251–5258, doi:10.1002/2014GL060868.

Received 11 JUN 2014
Accepted 1 JUL 2014
Accepted article online 8 JUL 2014
Published online 22 JUL 2014

A mechanism for future changes in Hadley circulation strength in CMIP5 climate change simulations

Kyong-Hwan Seo[1], Dargan M. W. Frierson[2], and Jun-Hyeok Son[3]

[1]Department of Atmospheric Sciences, Pusan National University, Busan, South Korea, [2]Department of Atmospheric Sciences, University of Washington, Seattle, Washington, USA, [3]Division of Earth Environmental System, Pusan National University, Busan, South Korea

Abstract The Coupled Model Intercomparison Project Phase 5 (CMIP5) 21st century climate change simulations exhibit a robust (slight) weakening of the Hadley cell (HC) during the boreal winter (summer, respectively) season in the future climate. Using 30 different coupled model simulations, we investigate the main mechanisms for both the multimodel ensemble mean changes in the HC strength and its intermodel changes in response to global warming during these seasons. A simple scaling analysis relates the strength of the HC to three factors: the meridional potential temperature gradient, gross static stability, and tropopause height. We found that changes in the meridional potential temperature gradients across the subtropics in a warming climate play a crucial role in the ensemble mean changes and model-to-model variations in the HC strength for both seasons. A larger reduction in the meridional temperature gradient in the Northern Hemisphere in boreal winter leads to the larger reduction of the HC strength in that season.

1. Introduction

Previous studies have shown an apparent weakening of the annually averaged Hadley cell (HC) under global warming in climate change model simulations [*Held and Soden*, 2006; *Lu et al*., 2007; *Ma et al*., 2012]. Overall, this is consistent with the prediction of a general slowdown of the tropical large-scale circulation due to a weakening of convective mass flux in a warming climate [*Held and Soden*, 2006]. *Ma et al*. [2012] proposed a slowdown of the tropical circulation in response to global warming due to the vertical advection of temperature anomaly by climatological mean vertical wind. As a result of increased dry static stability, anomalous cold (warm) advection appears in climatological ascending (descending) regions, opposing the climatological mean meridional circulation. General circulation model studies by *Levine and Schneider* [2011] and *Williamson et al*. [2013] showed that the Hadley circulation weakens as the meridional surface temperature gradients in the tropics and subtropics are reduced.

Relatively large model-to-model variations also exist in the strength of the HC. For example, the analysis of *Lu et al*. [2007] using 14 model simulations of the Coupled Model Intercomparison Project Phase 3 (CMIP3) indicates a multimodel mean annual weakening of ~1.2%/K with a range of ~0–4%/K. CMIP5 model data under the highest greenhouse gas emission scenario exhibit a similar per degree annual mean slowdown rate and intermodel variability (not shown).

The main mechanisms for future changes in the HC strength and its model-to-model variations have yet to be elucidated. The current study relates the multimodel ensemble mean and model-to-model variations in the HC strength with simple indices, using a scaling relation for Hadley cell strength as the basis. Since the winter HC is the stronger, we only focus on future changes in the winter HC intensity. So the analyses are performed on December-January-February (DJF) for the Northern Hemisphere (NH) and June-July-August (JJA) for the Southern Hemisphere separately. In order to investigate the major factors determining changes in the multimodel ensemble mean HC strength and the intermodel spread, two scaling theories are applied. These are both related to the width of the HC. The first argument is based on the near-inviscid theory for axisymmetric circulation without eddies, in which the axial angular momentum of poleward moving upper level air in the HC is assumed to be conserved [*Held and Hou*, 1980]. Then, the meridional width of the HC scales as $\phi_H \sim \left(\frac{gH\Delta_H}{\Omega^2 a^2}\right)^{\frac{1}{2}}$ [see also *Lu et al*., 2007]. Here H, the height of the tropopause, is estimated as the level at

which the temperature lapse rate decreases to 2°C km^{-1}. $\Delta_H = \frac{\theta_{eq} - \theta_{higher\ lat}}{\theta_0}$, which is the tropospheric mean meridional potential temperature gradient with θ_0 denoting the hemispheric troposphere mean potential temperature. The tropospheric mean is defined here as the average between 1000 and 400 hPa, where 400 hPa is chosen as the upper level to avoid stratospheric cooling over the high latitudes [*Frierson*, 2006]. Other parameters have their usual meanings in meteorology. From the thermodynamic equation and the mass continuity equation [*Vallis*, 2006], the meridional overturning stream function (ψ) of the circulation scales as

$$\psi \sim \left(\frac{gH\Delta_H}{\Omega^2 a^2}\right)^{\frac{3}{2}} \frac{aH\Delta_H}{\tau\Delta_V} \propto \frac{H^{\frac{5}{2}}\Delta_H^{\frac{5}{2}}}{\Delta_V}, \tag{1}$$

where τ is the characteristic overturning time scale of the circulation and $\Delta_V = \frac{\theta_{300} - \theta_{925}}{\theta_0}$, which is the dry static stability of the tropical troposphere.

The second theory involves the consideration of the baroclinically unstable shear appearing at the poleward edge of the HC [*Held*, 2000]. Here the HC width is set by the poleward extent of the angular momentum conserving circulation criterion until it breaks down by the baroclinically unstable vertical wind shear over the subtropics [see also *Lu et al*., 2007; *Kang and Lu*, 2012]. The width can be expressed as a function of the width in the first theory: ${\phi_{BC}}^4 = \frac{\Delta_V}{\Delta_H}{\phi_H}^2$ [*Held*, 2000]. There is no unique solution for the strength in the *Held* [2000] scaling, since one cannot satisfy both energy conservation within the cell and continuity of temperature with the radiative equilibrium profile at the cell edge with any solution other than the *Held and Hou* [1980] width. However, eddies would be expected to transport energy out of the cell and keep the temperatures at the cell edge away from radiative equilibrium, so we pursue a width scaling that satisfies neither of these constraints. We instead assume that the Held and Hou scaling for the velocity holds, so the strength change results only from modifications to the width. Then, the strength of the HC scales as

$$\psi \sim \left(\frac{gH\Delta_H}{\Omega^2 a^2}\right)^{\frac{5}{4}} \frac{H}{\tau} \left(\frac{\Delta_H}{\Delta_V}\right)^{\frac{3}{4}} \propto \frac{H^{\frac{9}{4}}{\Delta_H}^2}{{\Delta_V}^{\frac{3}{4}}}. \tag{2}$$

Its derivation can be seen in the Appendix A. The two scaling theories indicate that the HC strength is proportional to the tropopause height and equator-to-higher-latitude potential temperature gradient, but it is inversely proportional to gross static stability. A comparison of exponents suggests that the major contributions come from the meridional temperature gradient and/or the tropopause height, rather than the static stability. Although the tropopause height is related to the poleward expansion of the HC [*Lu et al*., 2007], we show later that its effect on the changes in the HC strength is insignificant.

2. Data Sets and Methods

In this study, the present climate is defined as the climate of the first 20 years (2001–2020) of the 21st century. For this, the historical simulation output from 2001 to 2005 was appended to the future warming scenario (see below) starting from 2006. The historical simulation was forced with changing atmospheric composition due to anthropogenic and volcanic influences, emissions or concentrations of short-lived species, natural and anthropogenic aerosols or their precursors, land use, and solar variability [*Taylor et al*., 2012].

For the climate projection, we used the representative concentration pathway (RCP) 8.5 scenario, which is the upper bound of the RCPs and does not include any specific climate mitigation target [e.g., *Riahi et al*., 2011]. The RCP 8.5 assumes that greenhouse gas emissions and concentrations increase considerably over time, leading to a radiative forcing stabilized at about 8.5 W m^{-2} at the end of the 21st century. The RCP 8.5 simulations for the 20 year period from 2081 to 2100 were used to represent the future climate. The first member of each ensemble was used in our analysis. All analyzed data are monthly mean data, and for ease of comparison, the data sets are interpolated into a 2.5° × 2.5° longitude-latitude grid. The 30 models we used are numbered in the following sequence in the plots: ACCESS1-0, ACCESS1-3, BCC-CSM1-1, BNU-ESM, CanESM2, CCSM4, CESM1-BGC, CESM1-CAM5, CMCC-CM, CNRM-CM5, CSIRO-Mk3-6-0, FGOALS-g2, FGOALS-s2, FIO-ESM, GFDL-CM3, GFDL-ESM2G, GFDL-ESM2M, HadGEM2-CC, HadGEM2-ES, INMCM4, IPSL-CM5A-LR, IPSL-CM5A-MR, MIROC5, MIROC-ESM-CHEM, MIROC-ESM, MPI-ESM-LR, MPI-ESM-MR, MRI-CGCM3, NorESM1-ME, and NorESM1-M.

The climate change response is defined as the difference between the first and last 20 years of the 21st century. The strength of the HC is determined by the zonally averaged mass stream function (ψ), which is

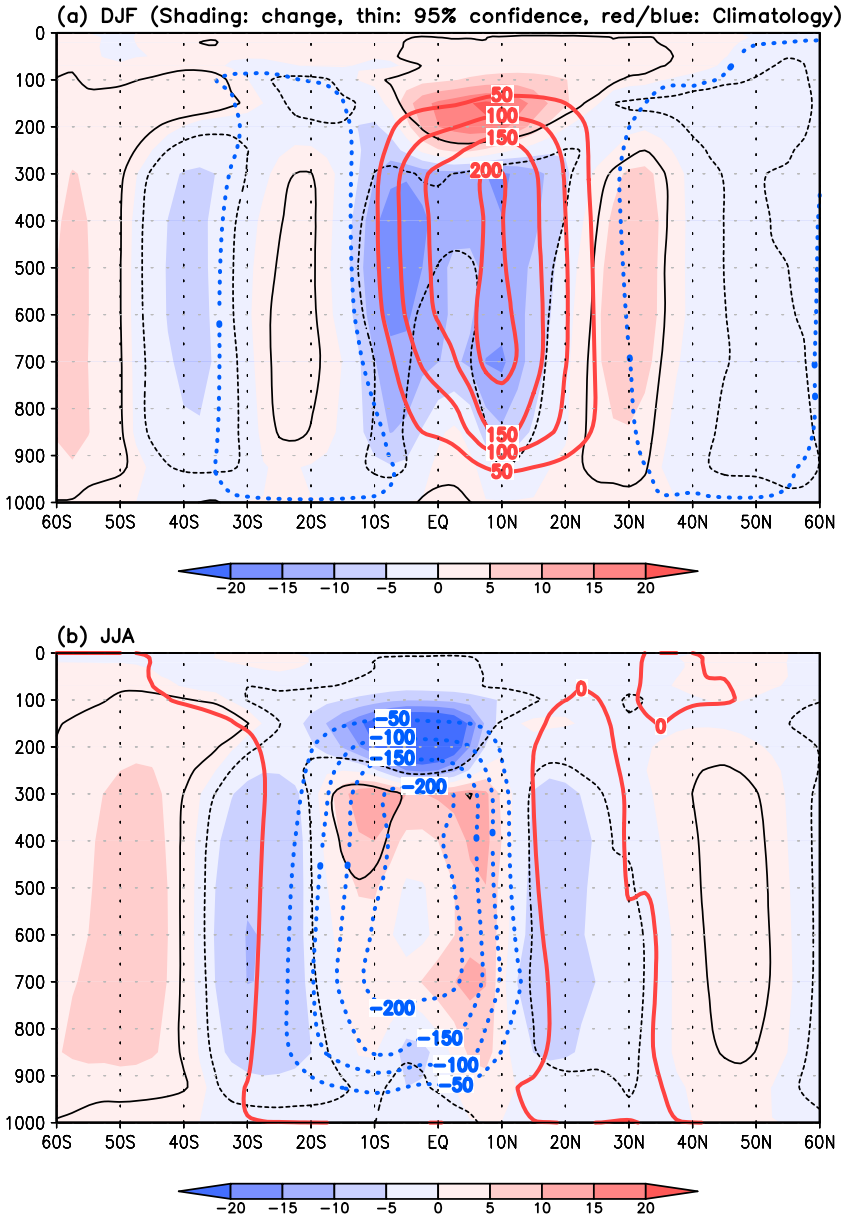

Figure 1. The 30 model ensemble mean stream function change (color shading, 10^9 kg s^{-1}) between the first and last 20 years of the 21st century during (a) DJF and (b) JJA. Thick contours denote the climatology of the present climate (i.e., the first 20 years of the 21st century). Thin lines represent the significant regions at the 95% confidence level based on the Student's *t* test. Positive stream function (thick red line) shows a clockwise circulation.

computed by vertically integrating the density-weighted zonal mean meridional wind from the top model level to the surface. The HC strength during DJF (JJA) is defined as the maximum (minimum, respectively) ψ over the tropics around 500 hPa. The use of the maximum (or minimum for JJA) ψ near 500 hPa or the difference between the values of the maximum and minimum ψ near 500 hPa over the tropics as an estimate of the HC strength does not significantly change the results.

3. Results

We first examine the change of the stream function over the tropics during DJF and JJA between the present climate and future climate in Figure 1. As shown in the figure, the negative stream function anomalies (shading) appear over (15°S, 15°N) during DJF (Figure 1a), indicating a significant weakening of the HC.

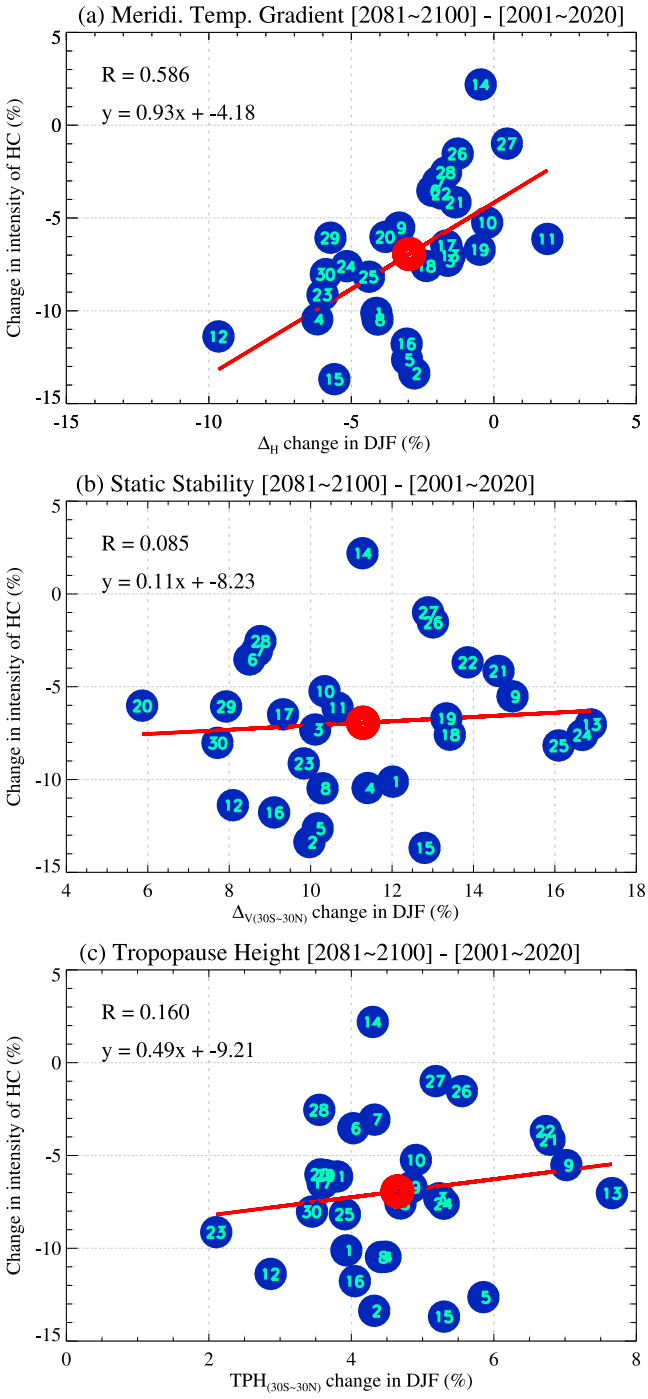

Figure 2. Changes in the intensity of the HC (%) against changes in (a) meridional potential temperature gradient measured as $\Delta_H = \frac{\theta_{[10°S-10°N]} - \theta_{[10°N-50°N]}}{\theta_0}$, (b) tropical static stability Δ_V and (c) subtropical tropopause height during DJF. Linear correlation coefficients and regression equations are shown in the plot.

The northward expansion of the wintertime cell is apparent. *Lu et al.* [2007] showed that this is caused by an increase in the subtropical static stability or tropopause height. Furthermore, due to the heightened tropical tropopause that results from increased warming in the tropical upper troposphere according to the moist adiabatic adjustment in a warming climate, the upward expansion of this cell is evident. However, the JJA stream function anomalies are less significant over the tropics (see contour in Figure 1b).

Figures 2 and 3 show changes in the HC strength for each model and their relationships with the three abovementioned candidate factors during DJF and JJA, respectively. The weakening of the HC is evident across almost all models during DJF (Figure 2a), whereas during JJA (Figure 3a), approximately half of the models predict a strengthening of the HC, while the other half exhibit a weakening, leading to a nearly negligible ensemble mean change in the strength of the HC for this period [*Ma and Xie*, 2013]. All models except for one (FIO-ESM) exhibit a weakening of the HC in DJF. The change in the HC strength is significantly correlated with the equator-to-higher-latitude difference in potential temperature across the winter hemisphere measured as $\frac{\theta_{[10°S-10°N]} - \theta_{[10-50°N]}}{\theta_0}$ (Figure 2a). Under a global warming scenario, almost all models (except for two) exhibit a larger increase in potential temperature over the subtropics and midlatitudes than over the deep tropics. Further, models with a more negative anomalous meridional temperature gradient have more weakening of the HC.

Tropical static stability (Figure 2b) and subtropical tropopause height (Figure 2c) during DJF both increase in all models. Changes in gross static stability or tropopause height, however, cannot explain the intermodel variability in the HC strength. We have also verified that the subtropical (20°N/S–40°N/S) static stability and subtropical tropopause height do not significantly correlate with intermodel changes in the HC intensity (r = 0.13–0.23). An increase in this subtropical static stability has been analyzed to be a primary cause of the poleward expansion of the HC [*Lu et al.*, 2007; *Frierson et al.*, 2007], as this pushes the baroclinically unstable zone poleward, thus moving the

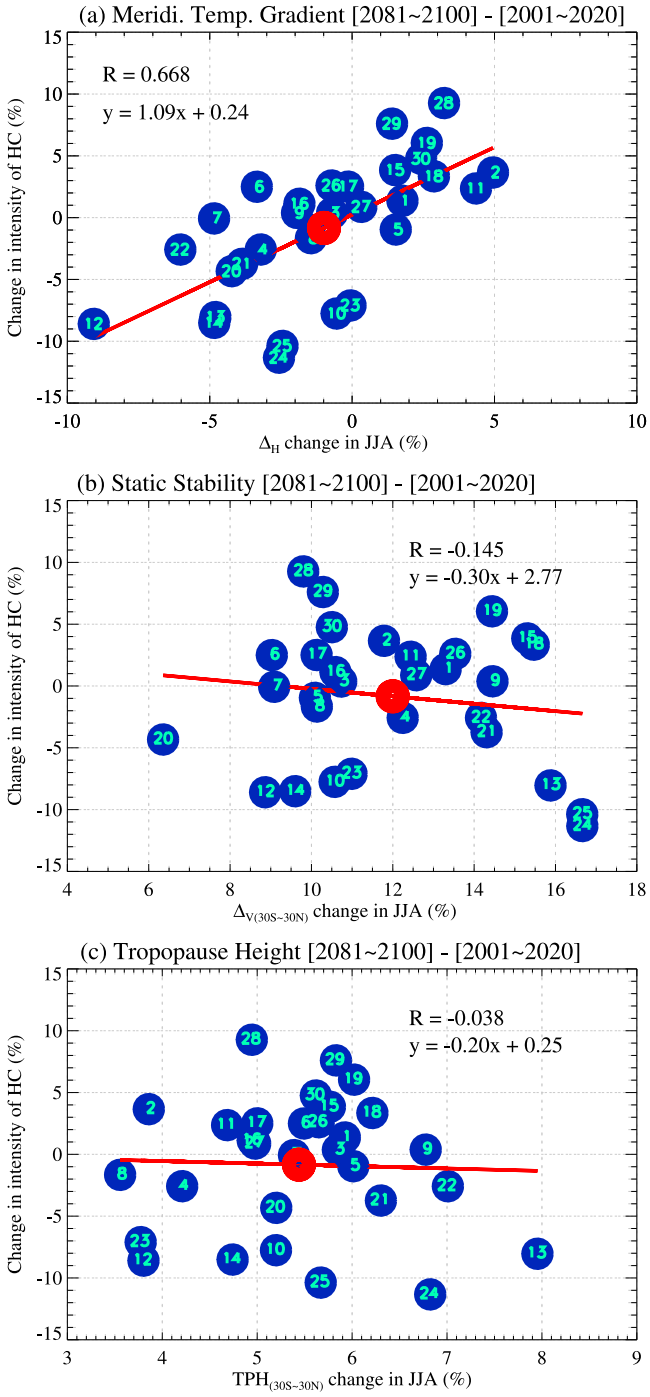

Figure 3. Same as Figure 2 except for the JJA HC (%). In Figure 3a, $\Delta_H = \frac{\theta_{[10°S\sim10°N]} - \theta_{[10°S\sim30°S]}}{\theta_0}$.

outer edge of the HC to higher latitudes. Again, the model-to-model variability with respect to the HC weakening is mainly related to the weakened meridional temperature gradient across the subtropics in response to global warming during this season.

Similar intermodel variations appear during JJA season (Figure 3): the HC intensity changes across models are highly correlated with changes in the meridional temperature gradient across the winter hemisphere defined as $\frac{\theta_{[10°S\sim10°N]} - \theta_{[10\sim30°S]}}{\theta_0}$ ($r = 0.69$), but these are not significantly correlated with changes in either static stability or tropopause height (Figures 3b and 3c). However, in contrast to the weakening tendency in the meridional temperature gradient in almost all models during DJF, in JJA there is a widespread scattering around zero. Models with decreased meridional temperature gradient slightly outnumber those with increased meridional gradient.

Modest changes in the higher-latitude boundary of the averaging region in the calculation of the latitudinal temperature gradients (i.e., 30°–50°N for DJF in Figure 2a and 10°–30°S for JJA in Figure 3a) do not change the results significantly for either season. The extratropical boundary of the averaging region was chosen objectively, from two different procedures. First, we calculated the correlation between trend-removed natural variations in the HC strength and meridional temperature gradient using the 21st century (100 year long) simulation data for each model with varied extratropical regions (from 25° to 55°) and chose the latitudinal domain that provided the maximum averaged correlation over all 30 models. This internal variability correlation reaches ~0.7 in some models. The second procedure was based on selecting a latitudinal extent with the largest number of models that satisfy the first relationship at the 1% significant level. An open question is why the DJF extratropical boundary is located farther poleward than corresponding value for JJA.

The multimodel ensemble mean changes in the HC strength (Figures 2 and 3) are fairly well predicted from the scaling relations. Denoting the future change as δ, then from the scaling relations (1) and (2), a percentage change in the HC strength can be expressed as follows: $\frac{\delta\psi}{\psi} \sim \frac{5}{2}\frac{\delta H}{H} + \frac{5}{2}\frac{\delta\Delta_H}{\Delta_H} - \frac{\delta\Delta_V}{\Delta_V}$ and $\frac{\delta\psi}{\psi} \sim \frac{9}{4}\frac{\delta H}{H} + 2\frac{\delta\Delta_H}{\Delta_H} - \frac{3}{4}\frac{\delta\Delta_V}{\Delta_V}$. Each component on the right-hand side of these equations can be seen in Figures 2 and 3. These two scaling

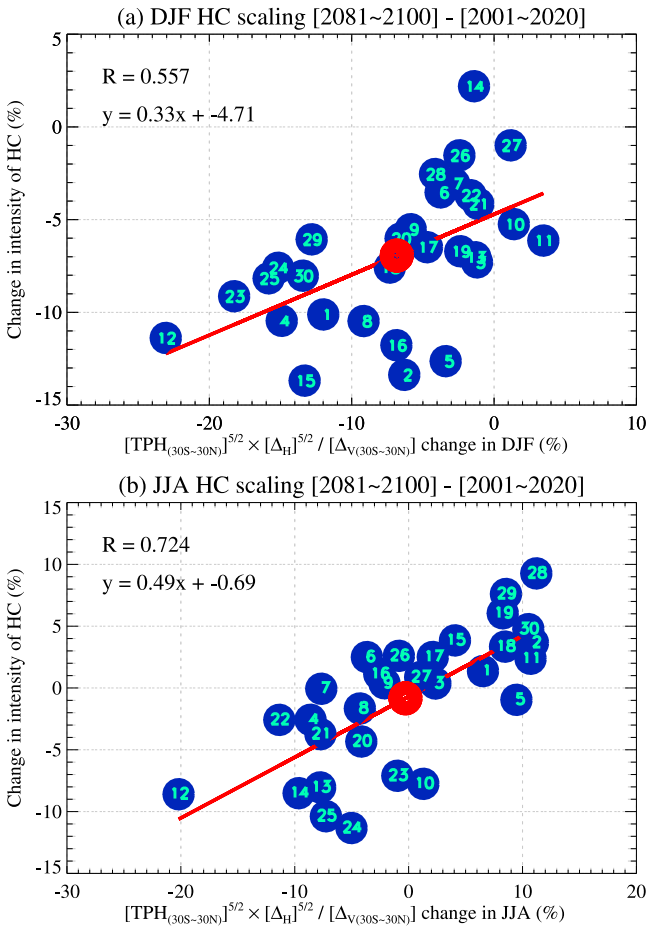

Figure 4. Changes in the intensity of the HC (%) during (a) DJF and (b) JJA according to the scaling equation (1).

relations give −6.9% and −3.7% for DJF and −1.2% and 0.9% for JJA, while the ensemble mean estimates directly from the model data are −6.9% for DJF and −0.8% for JJA, which are within the range that scaling relations predict. Since the changes in gross static stability and tropopause height in response to global warming are highly correlated (r = 0.95) (also in *Lu et al.* [2007]), the terms representing these two components cancel each other so their net effects on the percentage change in the HC strength are reduced. Considering this offsetting effect, we can scale the right-hand terms in equations (1) and (2) as $\psi \sim \Delta_H^{\frac{5}{2}} H^{\frac{3}{2}}$ and $\psi \sim \Delta_H^{2} H^{\frac{3}{2}}$, respectively, suggesting that the HC strength is more sensitive to Δ_H than H or Δ_V. Therefore, the dominant term in determining the ensemble mean HC strength change in the scalings comes from the ensemble mean change in the meridional temperature gradient.

Finally, we test the scaling arguments about the strength of the HC using data from each model. As shown in Figure 4, the intermodel spread in the changes of the HC intensity during both seasons is well aligned with changes in the right-hand side of equation (1) (the future change was calculated after initially computing the whole term on the right-hand side for current and future climates, separately). The correlation coefficient is 0.56–0.72, which is well above the 95% confidence level estimated by the Student t test. The scaling equation (2) gives a similar prediction to those in Figure 4. Note that while a zero crossing in the JJA scaling plot (Figure 4b) is evident, the DJF regression line intersects at a negative value in the ordinate. This suggests that there may be an additional factor causing the multimodel mean tendency to decelerate the HC in DJF. It may be associated with changes in the angular momentum of the winds [*Walker and Schneider*, 2006], or it may be associated with the NH having more zonal inhomogeneity due to the land/sea distribution compared to the Southern Hemisphere. It should be noted that removal of poorly performing models selected based on the performance of the internal HC dynamics as mentioned above gives rise to an improved prediction from the scaling theories (i.e., the intercept shifts more to the origin, not shown).

From the prediction of the scaling considerations and the current verification with CMIP5 data, it is concluded that change in the equator-to-higher-latitude temperature gradient in response to global warming is the most important factor in the determination of the future changes in both the ensemble mean HC strength and its intermodel variation.

4. Summary and Discussion

Thirty CMIP5 21st century climate change simulations show a robust weakening of the NH HC during the boreal winter season, while the boreal summer SH HC intensity exhibits a slight weakening in the future climate. The main factors affecting both the ensemble mean changes in the HC strength and its intermodel variability during these seasons have been investigated. A simple scaling analysis indicates that changes in

the HC strength are associated with changes in the meridional potential temperature gradient, gross static stability, and tropopause height. In contrast to the role that increased static stability and a heightened tropopause over the subtropics in a warming climate play on the poleward expansion of the HC [*Lu et al*., 2007; *Kang and Lu*, 2012], changes in the meridional potential temperature gradient are most important in explaining the multimodel ensemble mean changes in the HC strength with the significant weakening during DJF and the slight weakening during JJA. Furthermore, the model-to-model spread in the meridional potential temperature gradients explains the spread of the HC strength changes during both DJF and JJA. The scaling relations predict the characteristics of the ensemble mean and intermodel variations in the CMIP5 simulations fairly well.

Consistent with the role of the HC that transports a surplus of dry static energy poleward and, therefore, flattens the meridional temperature gradient, the decreased equator-to-higher-latitude temperature gradient in NH during DJF under global warming acts to decelerate the Hadley circulation. Even if the HC slows down in the future, more energy in the upper troposphere attained from the moist adiabatic process is expected to be transported poleward [e.g., *Hwang and Frierson*, 2010; *Zelinka and Hartmann*, 2012].

The question arises as to what controls the meridional temperature changes in a warming climate. An increase in the sea surface temperature over the subtropical and midlatitude oceans may be a major factor. Recent work by *Ma and Xie* [2013] suggests that intermodel variations of the sea surface temperature warming patterns regulate the changes in the annual mean HC weakening. Such changes may be interpretable with an energetic framework, as in *Frierson and Hwang* [2012]. On the other hand, a large increase in the land surface temperature in response to global warming may result in a large increase of the tropospheric temperature over the extratropics. In fact, the meridional temperature differences at these sea and land surfaces (instead of the tropospheric mean) significantly correlate to intermodel variations of the HC strength ($r = 0.4$–0.5, not shown).

In addition, since the reduced latitudinal temperature gradient in the projected future occurs across all latitudes during the NH DJF, we have tested the scaling arguments with a meridional temperature difference defined as an equator-to-pole gradient: $\Delta_H = \frac{\theta_{[10°S-10°N]} - \theta_{[70-90°N]}}{\theta_0}$. The same significant relationships appear as shown in Figures 2a and 4a. Therefore, polar amplification [e.g., *Manabe and Wetherald*, 1975] can be a source of the reduced meridional temperature gradient. All these factors should be examined in detail by performing sensitivity tests using general circulation models.

Appendix A: Derivation of Equation (2)

The strength of the HC can be expressed as

$$\psi \sim v_{BC} H,$$

where $v_{BC} \sim \frac{w}{H} Y_{BC}$ and Y_{BC} is the latitudinal extent of the HC. Therefore,

$$\psi \sim \frac{w}{H} Y_{BC} H \sim w Y_{BC} \sim w(a\varphi_{BC}).$$

Using *Held*'s [2000] scaling relation ${\phi_{BC}}^4 \sim \frac{\Delta_V}{\Delta_H} {\phi_H}^2$ and assuming that the *Held and Hou* [1980] scaling holds for velocity, the strength becomes

$$\psi \sim \left[\frac{5R\Delta_H}{18\tau\Delta_V} H\right] \left[a\left(\frac{\Delta_V}{\Delta_H} {\phi_H}^2\right)^{1/4}\right]$$

$$\sim \frac{5R\Delta_H}{18\tau\Delta_V} H a \left(\frac{\Delta_V}{\Delta_H}\right)^{1/4} {\phi_H}^{1/2}.$$

Since $R = \frac{gH\Delta_H}{\Omega^2 a^2}$ and $\phi_H = \left(\frac{5}{3}R\right)^{1/2}$, the intensity scales as follows:

$$\psi \sim \frac{H}{\tau}\left(\frac{\Delta_H}{\Delta_V}\right)^{3/4} R^{5/4}$$

$$\sim \frac{H}{\tau}\left(\frac{\Delta_H}{\Delta_V}\right)^{3/4} H^{5/4} {\Delta_H}^{5/4}$$

$$\sim \frac{H^{\frac{9}{4}} {\Delta_H}^2}{{\Delta_V}^{\frac{3}{4}}}.$$

Acknowledgments
We thank Jian Ma at University of Hawaii and Paulo Ceppi at University of Washington for their helpful comments. This work was funded by the Korea Meteorological Administration Research and Development Program under grant CATER 2012–3071, NSF awards AGS-0846641 and AGS-0936059. We would like to acknowledge the support from the Korea Institute of Science and Technology Information (KISTI). We acknowledge the World Climate Research Programme's Working Group on Coupled Modeling, which is responsible for CMIP, and we thank the climate modeling groups for producing and making available their model output.

The Editor thanks two anonymous reviewers for their assistance in evaluating this paper.

References

Frierson, D. M. W. (2006), Robust increases in midlatitude static stability in simulations of global warming, *Geophys. Res. Lett.*, *33*, L24816, doi:10.1029/2006GL027504.

Frierson, D. M. W., and Y.-T. Hwang (2012), Extratropical influence on ITCZ shifts in slab ocean simulations of global warming, *J. Clim.*, *25*, 720–733.

Frierson, D. M. W., J. Lu, and G. Chen (2007), Width of the Hadley cell in simple and comprehensive general circulation models, *Geophys. Res. Lett.*, *34*, L18804, doi:10.1029/2007GL031115.

Held, I. M. (2000), The general circulation of the atmosphere, *Proc. Geophysical Fluid Dynamics Program*, Woods Hole, MA, Woods Hole Oceanographic Institute, 1–70. [Available at http://gfdl.noaa.gov/cms-filesystem-action/user_files/ih/lectures/woods_hole.pdf.]

Held, I. M., and A. Y. Hou (1980), Nonlinear axially symmetric circulations in a nearly inviscid atmosphere, *J. Atmos. Sci.*, *37*, 515–533.

Held, I. M., and B. J. Soden (2006), Robust response of the hydrological cycle to global warming, *J. Clim.*, *19*, 5686–5699.

Hwang, Y.-T., and D. M. W. Frierson (2010), Increasing atmospheric poleward energy transport with global warming, *Geophys. Res. Lett.*, *37*, L24807, doi:10.1029/2010GL045440.

Kang, S. M., and J. Lu (2012), Expansion of the Hadley cell under global warming: Winter versus summer, *J. Clim.*, *25*, 8387–8393.

Levine, X. J., and T. Schneider (2011), Response of the Hadley circulation to climate change in an Aquaplanet GCM to a simple representation of ocean heat transport, *J. Atmos. Sci.*, *68*, 769–783.

Lu, J., G. A. Vecchi, and T. Reichler (2007), Expansion of the Hadley cell under global warming, *Geophys. Res. Lett.*, *34*, L06805, doi:10.1029/2006GL028443.

Ma, J., and S.-P. Xie (2013), Regional patterns of sea surface temperature change: A source of uncertainty in future projections of precipitation and atmospheric circulation, *J. Clim.*, *26*, 2482–2501.

Ma, J., S.-P. Xie, and Y. Kosaka (2012), Mechanisms for tropical tropospheric circulation change in response to global warming, *J. Clim.*, *25*, 2979–2994.

Manabe, S., and R. T. Wetherald (1975), Effects of doubling CO_2 concentration on the climate of a general circulation model, *J. Atmos. Sci.*, *32*, 3–15.

Riahi, K., S. Rao, V. Krey, C. Cho, V. Chirkov, G. Fischer, G. Kindermann, N. Nakicenovic, and P. Rafaj (2011), RCP 8.5—A scenario of comparatively high greenhouse gas emissions, *Clim. Change*, *109*, 33–57.

Taylor, K. E., R. J. Stouffer, and G. A. Meehl (2012), An overview of CMIP5 and the experiment design, *Bull. Am. Meteorol. Soc.*, *93*, 485–498.

Vallis, G. K. (2006), *Atmospheric and Oceanic Fluid Dynamics*, 745 pp., Cambridge Univ. Press, Cambridge, U. K.

Walker, C. C., and T. Schneider (2006), Eddy influences on Hadley circulations: Simulations with an idealized GCM, *J. Atmos. Sci.*, *63*, 3333–3350.

Williamson, D. L., et al. (2013), The Aqua-Planet Experiment (APE): Response to changed meridional SST profile, *J. Meteorol. Soc. Jpn.*, *91A*, 57–89.

Zelinka, M. D., and D. L. Hartmann (2012), Climate feedbacks and their implications for poleward energy flux changes in a warming climate, *J. Clim.*, *25*, 608–624, doi:10.1175/JCLI-D-11-00096.11.